Book of Tutorials and Abstracts

European Microbeam Analysis Society

EMAS 2024

14th

REGIONAL WORKSHOP

on

THE EDGE OF NEW EM AND MICROANALYSIS TECHNOLOGY

12 to 15 May 2024
at the
Brno University of Technology, Brno, Czech Republic

Organised in collaboration with:
Brno University of Technology (VUT)
Central European Institute of Technology (CEITEC)

EMAS
European Microbeam Analysis Society eV
www.microbeamanalysis.eu/

This volume is published by:
European Microbeam Analysis Society eV (EMAS)
EMAS Secretariat
c/o Eidgenössische Technische Hochschule, Institut für Geochemie und Petrologie
Clausiusstrasse 25
8092 Zürich
Switzerland

ISBN 978 90 8227 6978
NUR code: 971 – Materials Science

APPLICATION OF ELECTRON MICROSCOPY IN STEEL RESEARCH

Šárka Mikmeková

Czech Academy of Sciences, Institute of Scientific Instruments
Královopolská 147, 61264 Brno, Czech Republic
e-mail: sarka@isibrno.cz

Šárka Mikmeková received her BSc and MEng from Brno University of Technology, followed by an MSc from Masaryk University. In 2013 she obtained her PhD from Brno University of Technology with a thesis on "*Characterization of advanced materials with slow electrons*" for work done at the Institute of Scientific Instruments of the Czech Academy of Sciences in Brno. Subsequently, she worked for a number of years as a researcher at JFE Steel Corporation Steel research laboratory, Kawasaki, Japan. Since 2018, she is researcher and group leader of the research group "Microscopy for materials sciences" at the Institute of Scientific Instruments of the Czech Academy of Sciences in Brno, focussed on metallography, automatisation, robotics, optical and electron microscopy, materials characterisation, and machine learning.

1. INTRODUCTION

State-of-the-art scanning electron microscopes (SEMs) are equipped with sophisticated multiple detection systems consisting of various detectors situated not only in the chamber but also inside the tube. Simultaneous collection of micrographs from several detectors situated at different positions results in effective energy and angular filtering of the signal electrons based on their initial energy and emission angle. Effective filtering of the secondary electrons (SEs) and also the backscattered electrons (BSEs) enable us to optimise the desired contrast in the micrographs and diminish artefacts [1, 2]. Moreover, modern SEMs are equipped with a beam deceleration (BD) mode, which enables users to operate the commercial SEM at energies of tens or even units of eV. The principle of the BD mode is very simple [3]. The BD system consists of the cathode formed by a negatively biased specimen and the anode consisting of an earthed pole piece. The primary electrons are retarded in the electrostatic field to their final energy and the emitted electrons are collimated toward the optical axis and accelerated toward the detector. The BD mode enables us to observe the specimen surface at arbitrary low landing energies of the primary beam. Operating the SEM at very low landing energies results in a change in the physical picture of the contrast mechanism and electron-electron interaction becomes dominant. Despite the fact, that several interesting and promising contrasts in the SEM images obtained at low and super low landing energies have been reported [4-8], characterisation of industrial materials in the SEM at energies below 100 eV is still very rare. In this paper, selected applications of the low and super-low energy SEM in steel research will be presented.

2. FILTERING OF THE SIGNAL ELECTRONS

Secondary electrons originate from the surface or the near-surface region. SEs are a result of inelastic interactions between the primary beam electrons and the specimen and have energy below 50 eV. There are three types of SEs based on their origin namely SE1, SE2, and SE3. The SE1 are generated by the primary electrons, the SE2 are generated by the BSEs leaving the sample, and the SE3 are parasitic signal originating from the instrument chamber. As mentioned above, recent SEMs enable effective signal filtering. Figure 1 shows the SE micrographs of small oxide particles (Mn-B-O) on steel surfaces simultaneously obtained by various SE detectors. The detector A situated at the upper part of the tube collects the SEs with the lowest emission energy and emits close to the optical axis. In contrast, detector B collects also the low energy SEs but these electrons were emitted far from the optical axis. The last detector, i.e. detector C, is a conventional Everhart-Thornley detector situated in the chamber. The detector C collects the SEs having higher emitted energy, which left the specimen at the angles far from the optical axis. We have three different SE images offering different information about the specimen. Detector A shows information about chemical composition and the oxides appear darker than the matrix. The B detector offers information about surface degradation around the oxides and finally, the C detector brings common information about the topography.

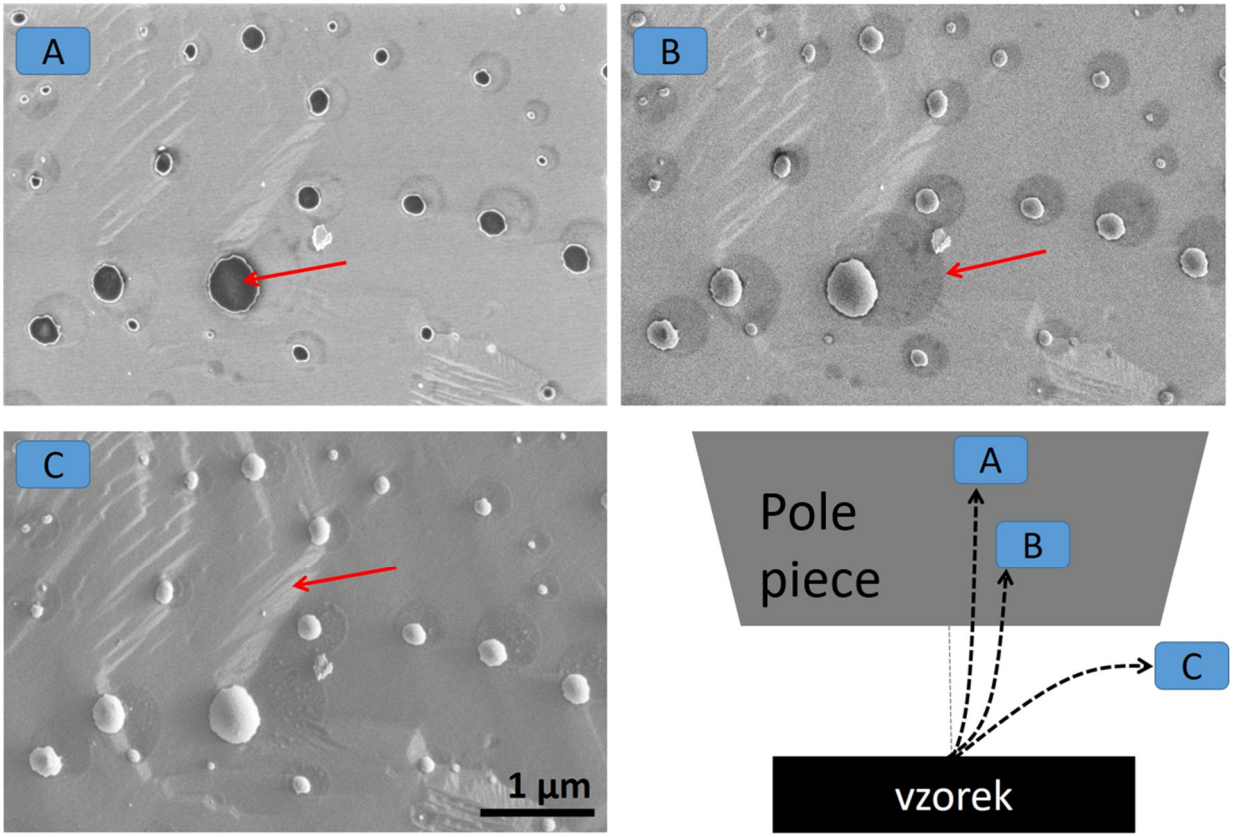

Figure 1. Energy and angular filtering of the SEs: Mn-B-oxides on a steel surface imaged by three different SE detectors.

State-of-the-art SEMs enable not only very effective SE signal filtering but also BSEs can be separated based on their initial energy which leaves the sample and the emission angle, as shown in Fig. 2. The four BSE images were collected simultaneously by each segment of a concentric back-scatter detector (CBS) situated below the pole piece. The imaged specimen is a steel containing carbides of iron and titan. Segment A is situated next to the optical axis and detects inelastically scattered low-energy BSEs emitted close to the optical axis. Segments B and C collect the signal created by the BSEs with energy close to the primary electrons (i.e., elastically scattered BSEs) and emitted far from the optical axis. Inelastic BSEs carry information about the material (so-called "Z" contrast) and segment A shows information about chemical composition. In contrast, the elastic BSEs are sensitive to crystallography and thus the segments far from the optical axis are more suitable for channelling contrast. The last segment, segment D, collects dominantly the electrons scattered under high angles from the optical axis and is extraordinarily sensitive to surface topography.

Insight into the extraordinary detection flexibility of modern multiple detection systems enables us to more effectively characterize material microstructure. Accurate knowledge about the signal received at each detector and the possibility of its modification can be successfully used for tuning of desired contrast or suppression of undesirable information.

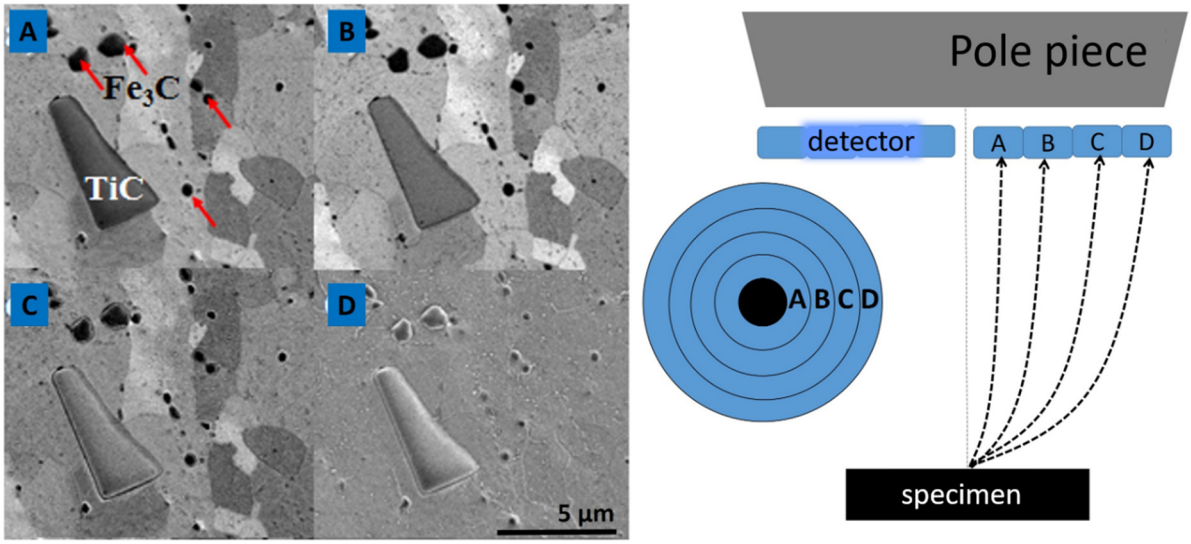

Figure 2. SEM BSEs micrographs simultaneously collected by individual segments of the CBS detector.

3. *MICROSCOPY WITH SLOW AND SUPER SLOW ELECTRONS*

The recent trend in scanning electron microscopy is to focus on using very low landing energies of the primary electrons. Operating the SEM at low and very low landing energy has several important benefits for imaging: High surface sensitivity, optimising of material contrast, non-charging microscopy – imaging of non-conductive specimens without covering of surface by a thin conductive layer, decreasing of radiation damage, etc. The dependence of interaction depth on the landing energy of the primary beam is demonstrated in Fig. 3. The interaction depth decreases with decreasing energy and high surface sensitivity is obtained at low 1 keV.

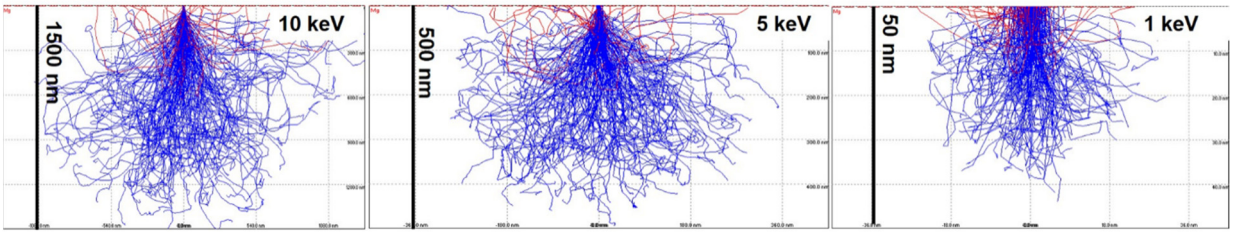

Figure 3. Monte-Carlo simulations of the electron trajectories into the Fe for a beam energy of 10, 5, and 1 keV (simulated with the CASINO software).

Using low landing energies is inseparably connected with increasing surface sensitivity, hence the surface conditions (e.g., presence/absence of native oxide, contamination, etc.) start to play a very important role in the image formation. Figure 4 shows a partially native oxide-covered steel surface (part of the native oxide was removed by in-situ ion beam cleaning) imaged at various landing energies of the primary beam in ultra-high vacuum (UHV) conditions.

As visible, the native oxide layer is invisible for higher energies and starts to be visible at 500 eV. At very low landing energies, say below 100 eV, the native oxide becomes impenetrable for primary electrons, and information about the steel substrate is lost.

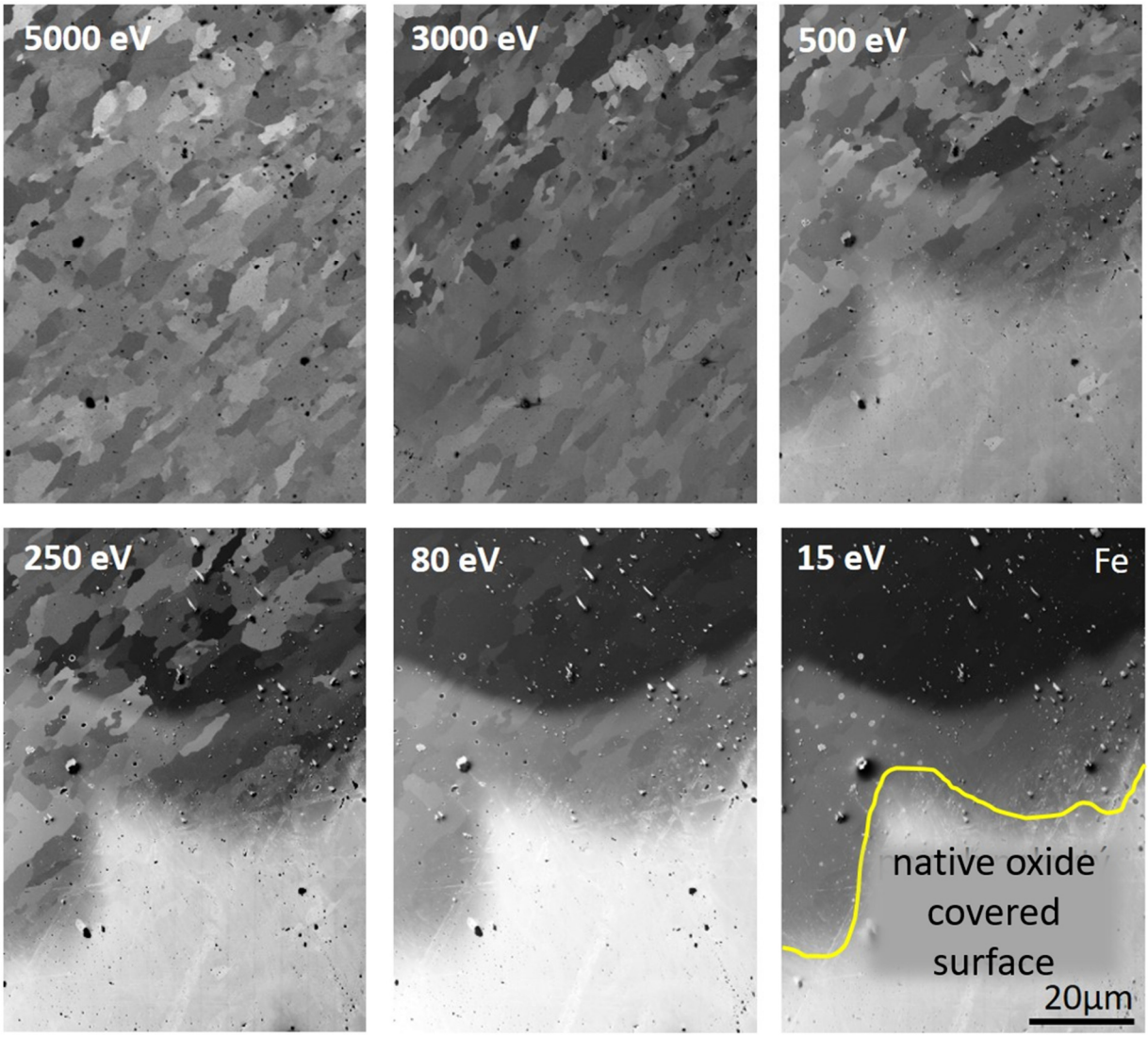

Figure 4. A series of the UHV low energy SEM micrographs of the same point of view obtained at landing energies from 5 keV up to 15 eV landing energy of the primary beam. Sample: Ferritic steel covered by native oxide layer.

4. SELECTED APPLICATIONS

In this part, selected applications of advanced SEM microscopic techniques, such as signal electron filtering and utilising slow and super slow electrons, will be presented. As mentioned above, the information depth decreases with decreasing landing energy of the primary beam.

Extreme surface sensitivity is obtained at tens of eV, where the inelastic mean free path (IMFP) reaches its minimum. At tens of eV, the information depth is only a few of Å. It makes the super low energy SEM a powerful tool for surface quality inspection. Figure 5 shows a steel surface covered with a protective film. Surface contamination in the form of small white circles is visible only at energies below 100 eV, i.e., area where the IMFP reaches its minimum.

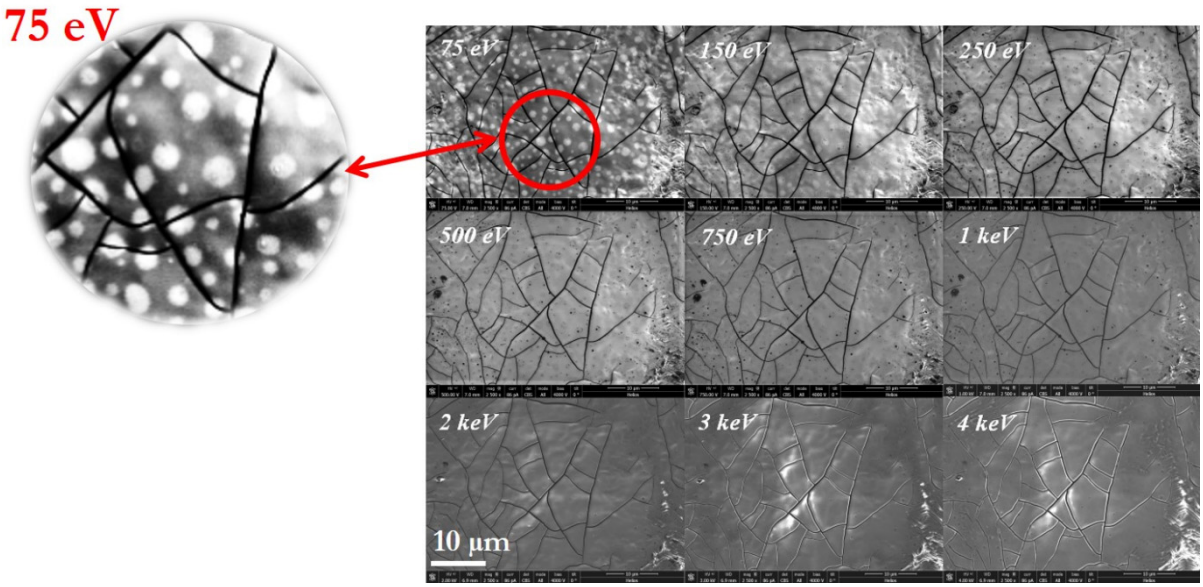

Figure 5. Steel surface covered by a protective Zn layer imaged at various landing energies of the primary electrons. Surface contamination becomes clearly visible at 75 eV.

Surface sensitivity at low landing energies is also useful for the inspection of fine surface features, such as fine Mn-B-oxides on steel surfaces. Figure 6 shows the same point of view imaged at energies from 100 eV up to 10 eV. The very small oxide particles become more and more visible with decreasing energy.

Modern SEMs can be operated at arbitrarily low landing energy. The landing energy of the primary beam is possible to continuously change employing a negative bias applied on a specimen surface. The information depth depends on the landing energy, which can be utilised for non-destructive 3D mapping, as shown in Fig. 7.

The following parts are focussed on the application of signal electron filtering in steel research. Figure 8 demonstrates the possibility of separation of carbides and Laves-phases utilising BSE signal filtering. The Cr-carbides and the Laves phases appear identical in contrast in the conventional non-filtered SEM images (Figs. 8a and 8b). The SEM images were obtained at 1 keV landing energy of the primary beam. Figure 8c was acquired at the same landing energy as the primary beam but the BSE detector collects only the low take-off angle BSEs. As visible,

it results in different contrasts, and the Laves phases become clearly visible and easily separable from the matrix and Cr-carbides.

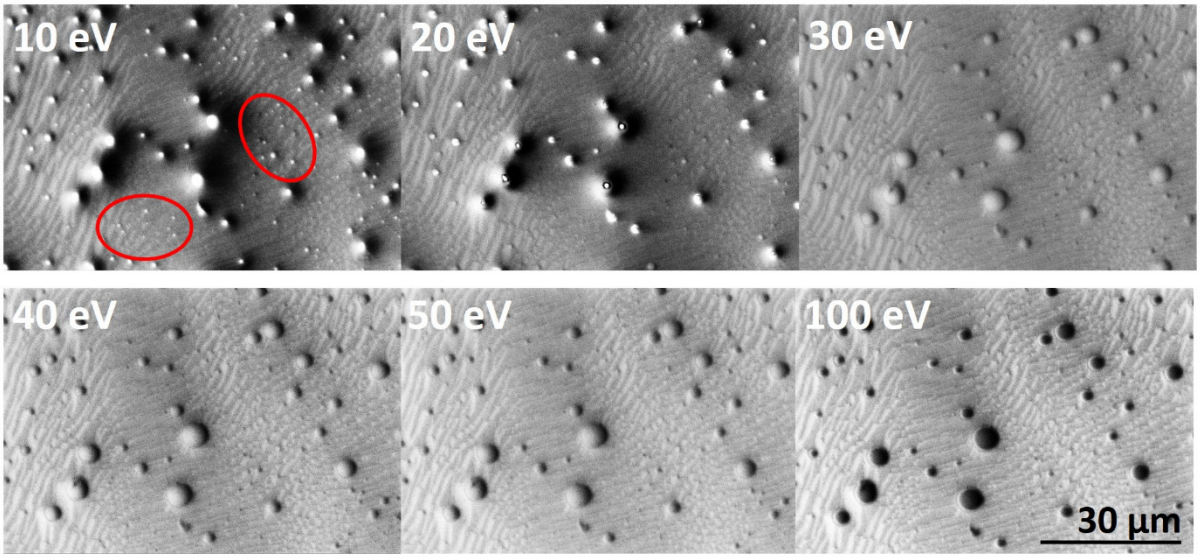

Figure 6. Steel surface covered by fine oxide particles imaged at various landing energies of primary beam.

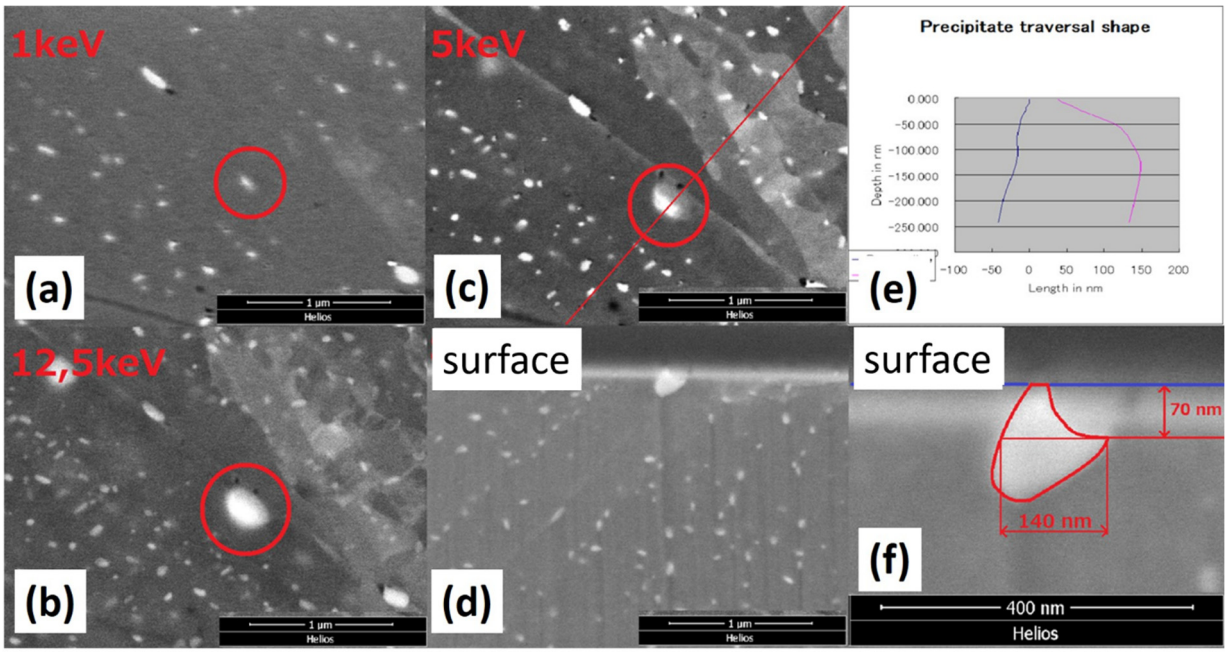

Figure 7. Non-destructive 3D mapping of precipitate situated on a grain boundary in steel. a) to c) SEM BSE images obtained at various landing energy of the primary beam; d) and f) Cross-section view; and e) Predicted shape of precipitate based on the SEM imaging.

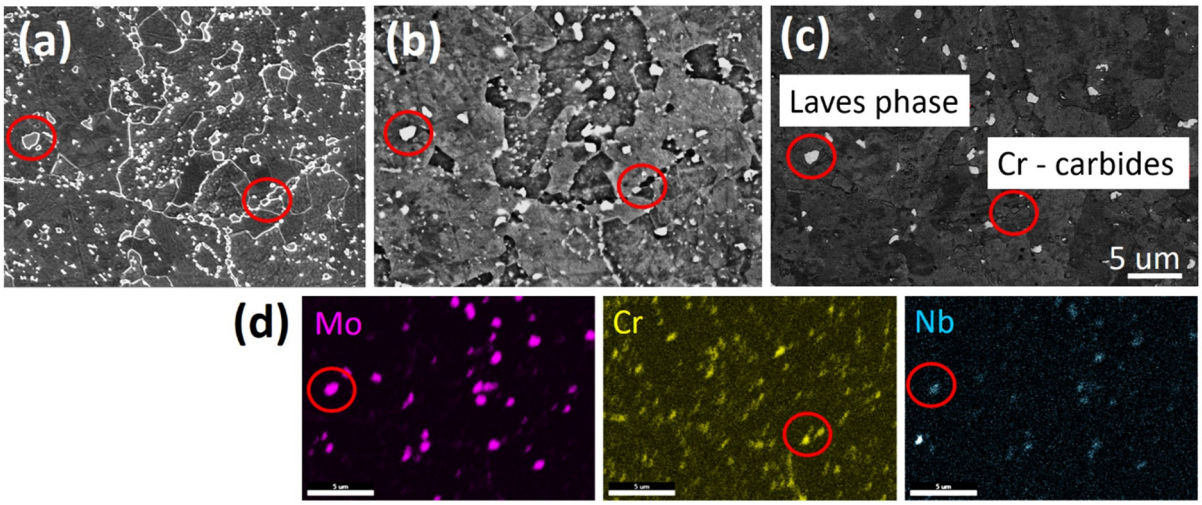

Figure 8. a) Conventional SEM SE micrograph; b) BSE micrograph of the COST F steel. c) Angular-filtered BSE image of the same area; d) Together with corresponding EDS maps of element distribution.

The next practical application of BSE signal filtering is a mapping of deformation-induced martensite (DIM) in austenitic steel. Figure 9 shows a) the conventional BSE image, and b the energy- and angular-filtered BSE image. As visible, the martensite phase exhibits a very bright contrast as a consequence of the high emission of signal electrons from this phase. The filtered image is created by in-elastically scattered BSEs. Extraordinary high emission of inelastic BSEs from the martensite phase is caused by a high density of defects, such as dislocations.

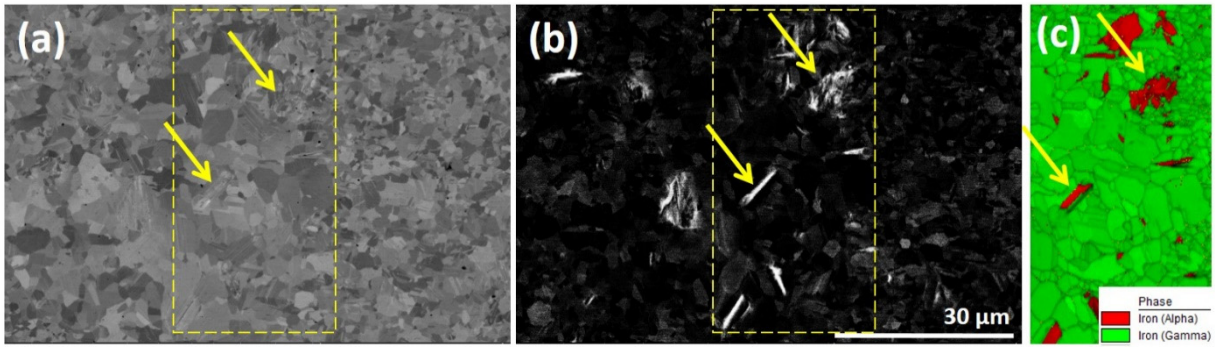

Figure 9. a) Standard SEM BSE image of the austenitic steel 301 LN containing DIM; b) Angular- and energy- filtered BSE image of the same point of view; and c) EBSD phase and IQ map confirming presence of martensite.

The last two figures, i.e., Figs. 10 and 11, demonstrate the benefits of the SEs filtering for the characterisation of advanced high-strength steels (AHSS). The AHSS has a complex

microstructure containing several different phases in-homogeneously distributed within a matrix. Figure 10 compares the conventional SE image of AHSS with the SE image of the same point of view obtained by the SE detector situated in the column. This detector collects very low energy SEs, i.e., true SEs, and precise information about the secondary phases is obtained. The secondary phases are visible and separable from the matrix. The prospect of the SE signal filtering for the separation of martensite and retained austenite phase is shown in Fig. 11.

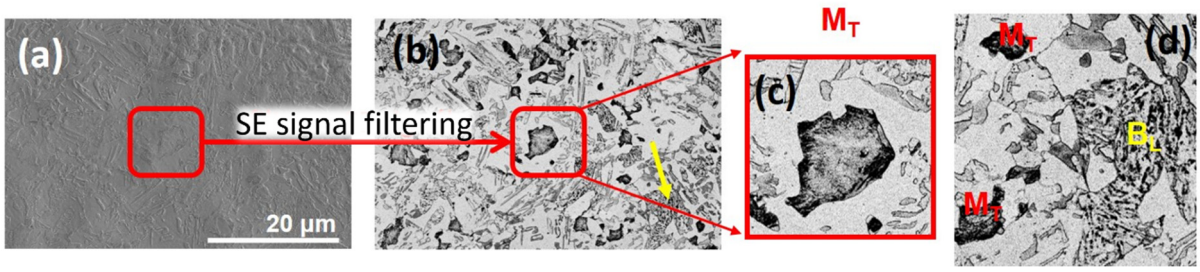

Figure 10. a) Standard SEM SE micrograph of AHSS and b) the low energy SE micrograph of same point of view.

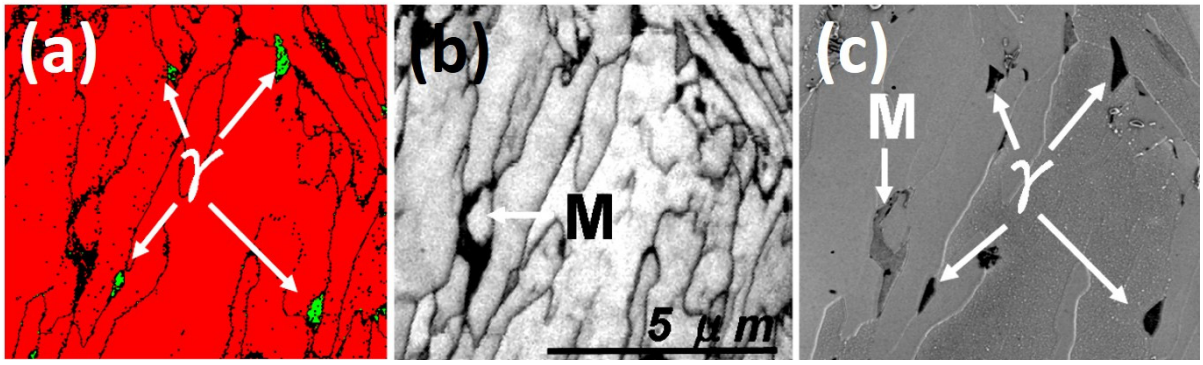

Figure 11. a) EBSD phase and b IQ maps of TRIP steel, together with c) SE-filtered image of the same point of view.

5. *CONCLUSION*

Modern scanning electron microscopes are equipped with sophisticated detection systems and enable to visualisation of a specimen surface at various landing energies of the primary beam. Signal electrons emitted from the specimen surface are effectively filtered based on their initial energy and emission angle. Filtering of the signal electrons enables us to optimise the desired contrast in the micrographs and suppress artefacts. Recent SEMs can be operated at energies from 30 keV up to tens of eV. This combination of detection flexibility together with the variability of landing energies of the primary electrons opens a new world of contrast mechanisms and enables more precise and accurate insight into the microstructure of advanced steels.

6. *REFERENCES*

[1] Mikmeková Š, Nakamichi H and Nagoshi M 2018 *Microscopy* **67** 11-17
[2] Mikmeková Š, Yamada K and Noro H 2015 *Microscopy* **64** 437-443
[3] Mikmeková Š, Yamada K and Noro H 2013 *Microscopy* **62** 589-596
[4] Aoyama T, Mikmeková Š, Hibino H and Okuda K 2019 *Ultramicroscopy* **204** 1-5
[5] Mikmeková Š and Aoyama T 2021 *Ultramicroscopy* **220** 113144
[6] Mikmeková Š, Aoyama T, Paták A and Zouhar M 2022 *Surf. Interface Anal.* **54** 667-676
[7] Aoyama T, Mikmeková Š and Kumagai K 2024 *Microscopy* 10.1093/jmicro/dfad042
[8] Mikmeková Š, *et al.* 2023 *Metals* **13** 1039